MetaSurface Structure Design and Channel Modelling for THz Band Communications

Luigi La Spada, Valeria Loscrì, Anna Maria Vegni

▶ **To cite this version:**

Luigi La Spada, Valeria Loscrì, Anna Maria Vegni. MetaSurface Structure Design and Channel Modelling for THz Band Communications. UBTCN'19 - Workshop on Ultra-high Broadband Terahertz Communication for 5G and Beyond networks in conjunction with IEEE INFOCOM 2019, Apr 2019, Paris, France. hal-02050843

HAL Id: hal-02050843

https://inria.hal.science/hal-02050843

Submitted on 27 Feb 2019

HAL is a multi-disciplinary open access archive for the deposit and dissemination of scientific research documents, whether they are published or not. The documents may come from teaching and research institutions in France or abroad, or from public or private research centers.

L'archive ouverte pluridisciplinaire **HAL**, est destinée au dépôt et à la diffusion de documents scientifiques de niveau recherche, publiés ou non, émanant des établissements d'enseignement et de recherche français ou étrangers, des laboratoires publics ou privés.

MetaSurface Structure Design and Channel Modelling for THz Band Communications

Luigi La Spada
School of Engineering and the Built Environment
Edinburgh Napier University
Edinburgh, United Kingdom
l.laspada@napier.ac.uk

Valeria Loscrí
FUN ResearchLab
INRIA Lille-Nord Europe
Lille, France
valeria.loscri@inria.fr

Anna Maria Vegni
Department of Engineering
Roma Tre University
Rome, Italy
annamaria.vegni@uniroma3.it

***Abstract*—Recently, a huge interest has been raised in controlling and manipulating electromagnetic waves by means of MetaSurfaces. This type of material makes possible the control of phase and amplitude of electromagnetic waves paving the way of different applications, like cloaking and communications in THz band.**

In this paper, we propose a novel approach for designing metasurface-based structures that are independent from the geometry and the frequency. As a proof of concept, we realize a 3D curvilinear metasurface and we show this approach can be effectively applied in different applications. In particular, for the THz-based system, we consider a transmitting antenna emitting a signal that impinges on the metasurface. Our analysis focuses on the evaluation of the attenuation of the incident signal on the metasurface in respect of characteristic design parameters, the length of the medium and the frequency.

***Index Terms*—metasurfaces, modeling, design, THz band, attenuation**

I. Introduction

In the last few years, there has been an increasing interest in the study of electromagnetic waves to manipulate their properties at will in different applications, such as telecommunications [1], [2], sensing [3], health [4], and automotive [5]. Different technologies and materials have been used to achieve this purpose, such as interferometers [6], miniaturized waveguides [7], gratings [8], [9], and the most recent 3D metamaterials. These materials show interesting advantages, but at the same time they need relatively large physical dimensions.

In this scenario a crucial role is played by metasurfaces *i.e.*, electromagnetic structures of arbitrary shape, composed of metallic and/or dielectric inclusions whose dimensions and periodicity are smaller compared to the operative wavelength. Metasurfaces can be implemented in different frequency ranges *i.e.*, microwave, mm-waves, THz, infrared and optics, and the main advantage in using such structures relies in the possibility to control their response through modeling, design and manufacturing [10] or via software [1], [2] for integration and miniaturization in existing platforms. Unfortunately, all such methods are valid for specific geometries, sources, and wave polarization. Until now, a generic approach able to link all the steps (*i.e.*, modeling, design, and manufacturing) is still missing. There is then the need to provide a method that allows the control of both amplitude and phase of the propagating electromagnetic wave independently of the geometry, the polarization and the frequency considered. Based on these considerations, we focus on the design of a technique with these specific features in order to be able to exploit the metasurface structure in different contexts.

Specifically, we propose the modeling, design of a metasurface able to control amplitude and phase of electromagnetic waves (independently of the frequency) and show its effectiveness for cloaking applications and for THz-band communications. In particular, we consider a communication system consisting of a transmitting antenna (*i.e.*, Tx antenna) that emits a signal impinging on the metasurface. In order to have a full control of the signal (*i.e.*, to control its amplitude and phase) and with the main objective of making the approach independent of the geometry and the frequency, the metasurface is characterized with inhomogeneities. This feature needs an accurate analysis of how the signal propagates along the metasurface, in order to be able to completely characterize the signal sent on-air. Based on these considerations, in this paper we evaluate the attenuation of a signal impinging on the above mentioned metasurface. In this work, we focus on THz band spectrum and will show the attenuation, both in respect of the characteristic parameters of the system, the distance (*i.e.*, length of metasurface) and the frequency of the signal.

The remainder of this paper is organized as follows. Section II describes the modeling and design of a given metasurface structure, characterized with its main geometrical and physical features. Specifically, through the use of the equivalent circuit-model theory, we will link the metasurface properties (*i.e.*, amplitude and phase found in the modeling section) with its physical characteristics (*i.e.*, inclusions' dimensions and spatial periodicity). In Section III, by means of non-homogeneous Transmission Line theory we will evaluate the wave-metasurface interaction in terms of amplitude and phase, thus deriving the attenuation expression, depending on both frequency and distance. Section IV presents numerical results that assess how the metasurface structure works in case of (*i*) cloaking and (*ii*) communications in the THz band. Specifically, we observe a dynamic behavior of the attenuation depending on the length of the metasurface and the frequency. This allows the opportune tuning of the geometrical

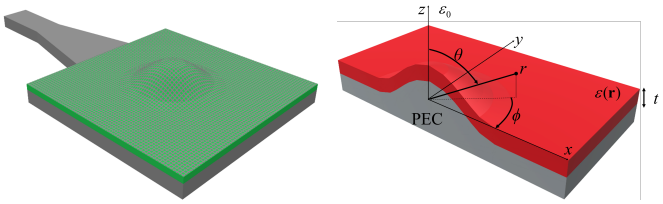

(a) (b)

Fig. 1. (a) Perspective view of a 3D curvilinear metasurface structure (*grey*) deposited on a grounded dielectric slab (*green*); (b) Side view and equivalent non-homogeneous permittivity model of the metasurface structure in spherical coordinate system (r, θ, ϕ).

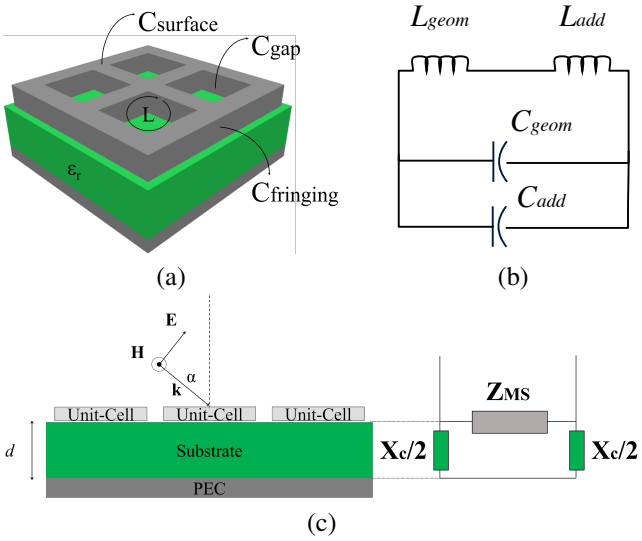

(a) (b) (c)

Fig. 2. (a) Square-cross particles as unit-cell; (b) its equivalent circuit-model: the non-homogeneity in the impedance profile is obtained by a variation of the geometrical parameters; (c) Non-Uniform Transmission Line model for the metasurface, resembling a Π-network.

and physical features of the metasurface in order to obtain the full control of the transmitted signal. Finally, conclusions are drawn at the end of the paper.

II. Metasurface Modeling and Design

In this section, we present a curvilinear metasurface-based structure, which will be considered in terms of its modeling and design.

Fig. 1(a) shows the geometry of a curvilinear metasurface formed by (metallic/dielectric) patches, printed on a grounded dielectric substrate. The substrate slab has thickness t, relative permittivity ε_{slab} and magnetic permeability $\mu_{slab} = \mu_0$, with μ_0 as the magnetic permeability of free space. The top layer is air with permittivity ε_0 and permeability μ_0, from where the wave impinges with an incident angle θ_i. Notice that it has been theoretically [11] and practically [12] demonstrated that electrically ultrathin metasurfaces cannot fully manipulate both amplitude and phase at the same time. For this reason, in this work the metasurface is considered to have finite and small thickness. With this assumption, we will demonstrate that a full control of the wave can be achieved.

Now, we aim to relate both amplitude and phase of the electric $\mathbf{E}$ (magnetic $\mathbf{H}$) wave components with the metasurface impedance $\mathbf{Z}$.

The structure of Fig. 1(a) can be considered as a slab with non-homogeneous constitutive parameters such as electric permittivity $\varepsilon(\mathbf{r})$ and/or magnetic permeability $\mu(\mathbf{r})$, function of the position vector $\mathbf{r}$, as also shown in Fig. 1(b). To model the electromagnetic behavior of the structure we will make use of both Maxwells' and Heltmotz equations. It is well-known that the solution of such equations in homogeneous materials is very straightforward. On the other hand, in non-homogeneous media such an equation became more complex. Let us consider the structure being electrically non-homogenous $\varepsilon(\mathbf{r})$ and magnetically homogeneous $\mu_r = \mu_0$. The electric $\mathbf{E}$ and magnetic $\mathbf{H}$ vector equations read, respectively:

$$\nabla^2 \mathbf{E} + \nabla \left[\mathbf{E} \bullet \nabla \log Z(\mathbf{r}) \right] + \omega^2 Z(\mathbf{r}) \mathbf{E} = 0, \quad (1)$$

and

$$\nabla^2 \mathbf{H} + \nabla \log Z(\mathbf{r}) \times (\nabla \times \mathbf{H}) + \omega^2 Z(\mathbf{r}) \mathbf{H} = 0, \quad (2)$$

where $Z(\mathbf{r})$ is the non-homogeneous impedance profile for the metasurface, expressed as [13]

$$Z(\mathbf{r}) = [Z_r, Z_\theta, Z_\phi] = \left[\frac{\pi}{\pi - 2r^2}, \sin^2(\theta), \frac{1}{\varepsilon_r} \right]. \quad (3)$$

It is known that both electric $\mathbf{E}$ and magnetic $\mathbf{H}$ vectors can be expressed in terms of amplitude $A(\mathbf{r})$ and phase $\Phi(\mathbf{r})$ as $\mathbf{E}(\mathbf{r}) = A_e(\mathbf{r}) e^{j\Phi_e(\mathbf{r})}$ and $\mathbf{H}(\mathbf{r}) = A_m(\mathbf{r}) e^{j\Phi_m(\mathbf{r})}$, respectively. By using non-homogeneous Transmission Line theory, we can link them to the structure impedance $Z(\mathbf{r})$ as follows [13]:

$$A(\mathbf{r}) = \left| \frac{Z(\mathbf{r}) - Z_0}{Z(\mathbf{r}) + Z_0} \right|, \quad (4)$$

and

$$\Phi(\mathbf{r}) = k_0 \int \frac{\sqrt{\mu_r}}{Z(\mathbf{r})} d\mathbf{r}, \quad (5)$$

being $Z_0 = 377\Omega$ the free-space impedance, and $k_0 = 2\pi/\lambda_0$ the free space wave-number. Eq. (4) and (5) establish the link between wave amplitude $A(\mathbf{r})$ and phase $\Phi(\mathbf{r})$ with the metasurface impedance $Z(\mathbf{r})$.

Finally, we aim to express the link of the metasurface impedance $Z(\mathbf{r})$ with its physical dimensions (*i.e.*, geometry, shape, volume, length, periodicity). Let us consider a square/crossed-shape patch as a unit-cell deposited on a grounded dielectric (*i.e.*, ε_r) substrate as depicted in Fig. 2(a). To evaluate the total impedance of the structure, three main steps have to be undertaken:

1) **Unit-cell**: when an electromagnetic wave impinges on the structure of Fig. 2(a), a time-varying magnetic ($\mathbf{H}$) component in the direction perpendicular to the surface of the unit-cell arises. In addition, a small electric ($\mathbf{E}$) component along the gap exists. Consequently, along the surface, different types of currents are induced *i.e.*, the electric $\mathbf{J_e} = \mathbf{n} \times \mathbf{H}$, magnetic equivalent $\mathbf{J_m} = -\mathbf{n} \times \mathbf{E}$ and electric displacement $\mathbf{J_d} = \varepsilon \mathbf{E}$. The unit-cell will

be equivalent to a shunt impedance composed by a reactance X_{MS} of inductive $X_L(\mathbf{J_m}) = j\omega L$ or capacitive $X_C(\mathbf{J_d}) = 1/j\omega C$ nature, if the structure is metallic or dielectric, respectively. Its circuit model is shown in Fig. 2(b), and the related Impedance reads as [14]:

$$Z_{unit-cell} = \frac{\int_a^b \mathbf{E}(\mathbf{r}) \bullet d\mathbf{l}}{\int_C \mathbf{H}(\mathbf{r}) \bullet d\mathbf{l}}, \tag{6}$$

where $\mathbf{E}(\mathbf{H})$ are the electric (magnetic) vectors along the structure, l is the line element, a and b the points of electric potential, and C is the magnetic closed loop.

2) **Thickness**: if the metasurface has a finite thickness, especially at frequencies such as THz/Infrared, additional electric ($\mathbf{J_{d-add}}$) and/or magnetic ($\mathbf{J_{m-add}}$) energy is stored within the metal, corresponding to an inductive $X_{add}(\mathbf{J_{m-add}}) = j\omega L_{add}$ and/or capacitive $X_{add}(\mathbf{J_{d-add}}) = 1/j\omega C_{add}$ reactance, respectively. Such additional terms are contained in the circuit model of Fig. 2(b), and their expressions can be found in [15]. In addition, if the metasurface is deposited on a dielectric substrate, electric displacement currents $\mathbf{J_{d-sub}}$ are present. It is equivalent to a series capacitive reactance $X_C(\mathbf{J_{d-sub}}) = 1/j\omega C_{sub}$ as shown in the Transmission Line model of Fig. 2(c).
3) **Coupling phenomena**: in our design, the unit-cells are arranged so close to each other like a net, leading to a highly confined field among adjacent particles. In this case, the adjacent structures result magnetically Z_L and/or electrically Z_C coupled due to the presence of both an (inductive) magnetic field $\mathbf{B} = \mu\mathbf{H}$ and/or a (displacement) electric field $\mathbf{D} = \varepsilon\mathbf{E}$ across the unit-cells, respectively.

A metasurface structure that includes parallel and/or series impedance elements, in the form of a Π- or T-network as that one presented in this paper (see Fig. 2(c)), allows us the full control of both amplitude and phase of the propagating electromagnetic wave:

$$Z = Z_{unit-cell}//X_c//Z_M. \tag{7}$$

III. Non-Homogeneous Transmission-Line model

The proposed metasurface structure can be described by its equivalent Non-Homogeneous Transmission Line (TL) model along the radial, angular and azimuthal directions *i.e.*, (r, θ, ϕ), respectively as:

$$\begin{cases} \dfrac{\partial V_1(r)}{\partial r} = -Z_r(r) I_1(r) \\ \dfrac{\partial I_1(r)}{\partial r} = -Y_r(r) V_1(r) \\ Z_r(r) = \dfrac{\pi}{\pi - 2r^2} \end{cases} \tag{8}$$

$$\begin{cases} \dfrac{\partial V_2(r)}{\partial \theta} = -Z_\theta(\theta) I_2(\theta) \\ \dfrac{\partial I_2(\theta)}{\partial \theta} = -Y_\theta(\theta) V_2(\theta) \\ Z_\theta(\theta) = \sin^2(\theta) \end{cases} \tag{9}$$

and

$$\begin{cases} \dfrac{\partial V_3(\phi)}{\partial \phi} = -Z_\phi(\phi) I_3(\phi) \\ \dfrac{\partial I_3(\phi)}{\partial \phi} = -Y_\phi(\phi) V_3(\phi) \\ Z_\phi(\phi) = \dfrac{1}{\varepsilon_r} \end{cases} \tag{10}$$

where $V_{1,2,3}$ and $I_{1,2,3}$ are the voltages and the currents in the i-th TL with $i = [1, 2, 3]$, and $Y(\mathbf{r}) = [Y_r, Y_\theta, Y_\phi]$ are the components along (r, θ, ϕ) of the TLC admittances.

For each TL, the related power transfer function can be evaluated. For telecommunications applications, we are interested in solving the TL equation along the radial direction r.

We first assume the voltage along r as follows:

$$V_1(r) = a_1 e^{-\alpha r} + a_2 e^{\alpha r}, \tag{11}$$

where the first term represents the propagating wave and the second term the reflected one. Specifically, $a_{1,2}$ are the amplitudes of the waves and α is the complex wavenumber. Let us assume that voltage and current at the beginning and end of the line of length d [m] are, respectively (V_0, I_0) and (V_d, I_d). Then, the power transfer function out-in along the radial direction easily reads as:

$$\frac{P_{out}}{P_{in}} = \frac{4e^{-(\alpha+\alpha^*)r}}{Z_r(r)} \left[\frac{|\zeta|^2}{(1+\zeta)^2 - (1-\zeta)^2 e^{-4r\alpha}} \right], \tag{12}$$

where the symbol * is for the conjugated operator, $Z_r(r)$ is defined in Eq. (8), and also we have defined

$$\zeta = -\frac{Z_{load}}{Z_r(r)}, \tag{13}$$

with Z_{load} as the load impedence. Similar results apply for the TL along the other directions, *i.e.*, angular and azimuthal, respectively.

From Eq. (12), we can easily compute the attenuation as a function of the distance d of the TL *i.e.*,

$$L(d) = -10 \log \left(\frac{P_{out}}{P_{in}} \right). \tag{14}$$

On the other hand, by explicating Z_{load} as composed by an inductive and/or capacitive nature, we can observe the attenuation behavior as dependent on the frequency *i.e.*,

$$Z_{load} = R + j\omega L + \frac{1}{j\omega C}, \tag{15}$$

with $\omega = 2\pi f$ as the frequency.

IV. Results and Discussion

We are going now to use the proposed approach to model, design and realize a curvilinear metasurface for two applications *i.e.*, (*i*) cloaking to blind objects for invisible applications and (*ii*) for THz-band communications.

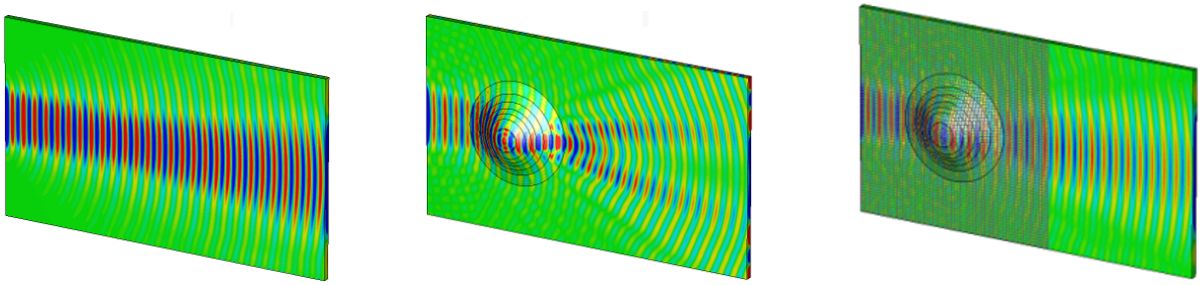

(a) (b) (c)

Fig. 3. 2D plot normal component of electric field E_z for: (a) Flat plane (RS), (b) curved object with uniform dielectric layer (No-Cloak) (c) the object with non-homogenous metasurface (Cloak).

A. Cloaking Application

The structure under study consists of a 3D curvilinear metasurface, where the metallic object used to retransmit the impinged signal is placed underneath (see Fig. 1). The metasurface consists of metallic particles deposited on a dielectric substrate of homogeneous permittivity ε_r, acting as substrate (see Fig. 2). In this case, the position vector $\mathbf{r}$ can be described by using the spherical coordinate system (r, θ, ϕ). The excitation is provided by a pyramid horn antenna whose has a well-known electromagnetic configuration, *i.e.*,

$$E\left(r,\theta,\phi\right) = a_{mn} H_n^m\left(\beta_d r\right) P_n^m\left(\cos\theta\right) \sin\left(m\phi\right). \qquad (16)$$

To practically realize the metasurface impedance $Z(\mathbf{r})$, in the design step, we need to discretize the continuous distribution along the radial r, angular θ and azimuthal Φ, directions by properly varying dimensions and shape of the inclusions (see Fig. 2). By using Eq. (6), the impedance of the unit-cell reads as

$$Z_{unit-cell} = \frac{j\omega L_{tot}}{1-\omega^2 L_{tot} C_{tot}}, \qquad (17)$$

where the inductance L_{tot} and capacitance C_{tot} can be related to the metasurface physical dimensions (*i.e.*, length l, width w, gap g and thickness t [m]), as follows:

$$L_{tot} = 4L_{self}\left(l,\omega,t\right) - 4M\left(l, l-\omega\right), \qquad (18)$$

with L_{self} the self-inductance of the loop and M the mutual inductance between the three-dimensional arms of the single unit-cell, and

$$C_{tot} = C_g\left(\omega,g,t\right) + C_f\left(l,\omega,g\right) + C_s\left(l,\omega,g,t\right), \qquad (19)$$

being C_g the capacitance for the electric field lines in the gap/slot parallel plates, C_f related to the fringing electric field across the arms, and C_s describes charges along the ring surface [15].

In terms of manufacturing, the Impedance distribution value can be achieved by using materials and fabrication techniques well established in literature. The performance results of the realized structure are depicted in Fig. 3. Three different samples are considered *i.e.*, (*i*) a flat grounded dielectric slab with homogeneous permittivity as reference, (*ii*) the object under an homogeneous permittivity layer as no-cloak, and (*iii*) the object covered with the realized metasurface as cloak. All different samples are depicted in Fig. 3.

The three samples have equivalent planar dimensions (*i.e.*, 140×140 mm^2), and dielectric layer thickness (*i.e.*, 4.5 mm). The 3D curvilinear surface has height equal to 17.1 mm. More specifically, for the uniform dielectric slabs, planar and curved, the permittivity value (*i.e.*, $\varepsilon_r = 15$) have been achieved by using dielectric mixtures with different volume fractions and particle sizes as in [13].

To evaluate the performance of each sample, we plot amplitude and phase of the normal electric field component E_z along the plane xy. A spectral analysis has been used to decompose the complex signals into simpler parts by applying Fourier transform. The analysis consists in the following steps *i.e.*, (*i*) Fourier transform from spatial domain to frequency spatial domain, (*ii*) filtering and isolation of surface wave component in the bi-dimensional spatial frequency spectrum, and (*iii*) surface wave conversion in the spatial domain to obtain the field distribution of the electric field that only contains the surface wave.

As reference for our evaluation, the flat plane case is considered, where the field is propagating undisturbed and the electric field has a well-known configuration, as depicted in Fig. 3(a). On the other hand, for the uniform 3D curvilinear surface case, in Fig. 3(b) we note a large amount of forward wave scattering, or electromagnetic shadow, caused mostly by interference patterns in the area after the object. Finally, when the metasurface structure is implemented, the wave is guided properly along the interface with no shadow left behind, as the obstacle is cloaked, as shown in Fig. 3(c).

B. TeraHertz Communication

Concerning the second application related to the communications in the THz band, recent results have been carried out in metamaterials with chiral features [16]. Now, in this paper we consider a system model with a transmitting antenna feeding the metasurface structure through an impinging signal. The signal propagates along the radial direction and the reflected signal will then be transmitted on air toward a receiver. In such a scenario, our aim is to control the features of the emitted signal, in terms of amplitude and phase. The behavior

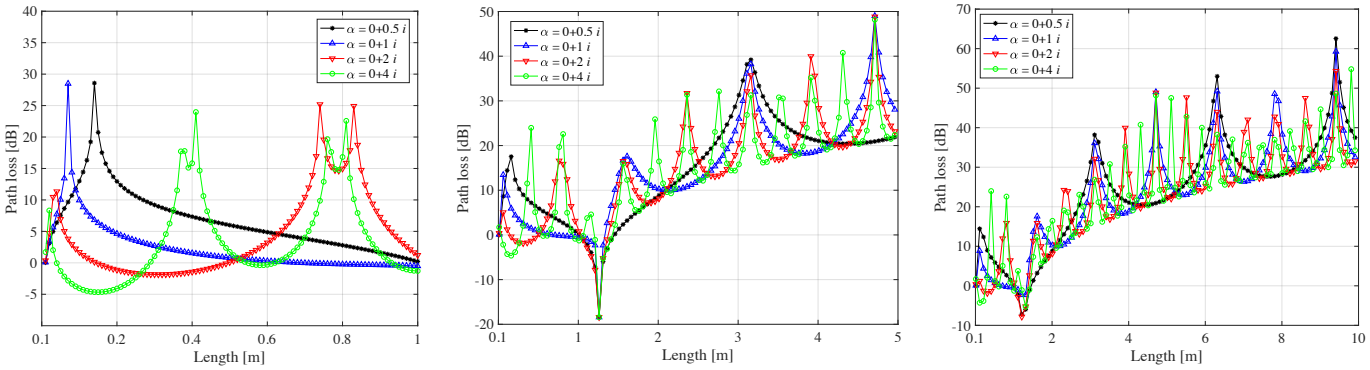

Fig. 4. Attenuation [dB] behavior for different values of α, in case of Transmission-Line length of (a) 1 m, (b) 5 m and (c) 10 m.

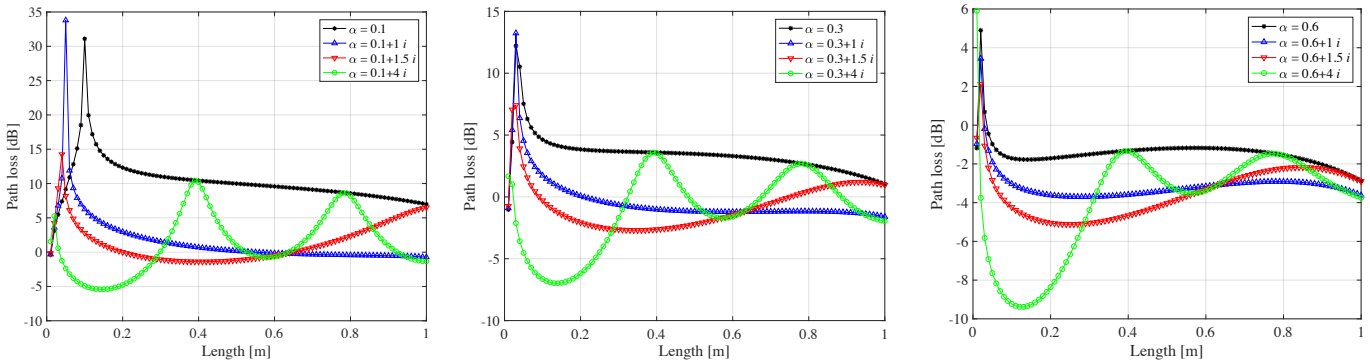

Fig. 5. Attenuation [dB] behavior in case of Transmission-Line length of 1 m for (a) $\mathrm{Re}[\alpha] = 0.1$, (b) $\mathrm{Re}[\alpha] = 0.3$, and (c) $\mathrm{Re}[\alpha] = 0.6$.

of the attenuation at the output of the metasurface allows to understand how the emitted signal can be controlled.

As follows, we show the numerical results of the signal behavior traveling along the metasurface presented above. Our evaluation is based on the impact of the parameter α on the signal propagation in respect of the length of the metasurface and the signal frequency. Fig. 4 depicts the attenuation [dB] versus the Transmission-Line length r [m] and different values of α *i.e.*, $\alpha = [0.5, 1, 1.5, 2]i$. We notice some peaks and fluctuations of the attenuation caused by the inhomogeneity of the medium. Specifically, for short length of the propagation medium as in Fig. 4(a), we observe a smoother behavior of the attenuation, characterized by peaks at very short distances followed by an attenuation of the propagated signal. Moreover, we observe other secondary peaks occurring for increasing lengths and higher values of α, both in real and imaginary parts of α.

The behavior of attenuation becomes richer of fluctuations when we observe a channel of higher length, as the case of Fig. 4(b). The dynamic of attenuation has an increasing trend with the length of the metasurface, thus meaning that longer the channel, higher the loss. However, we also notice that the behavior is not linear with the length, but it is a kind of periodic trend, with peaks followed by minimums (*i.e.*, wave-function behavior). This feature is easily noticeable in Fig. 4(c), where we observe the attenuation in case of a 10 m propagation medium. Finally, we remark that in Fig. 4(b) for a length of ≈ 1.2 m, the attenuation shows a negative value (*i.e.*, ≈ -20 dB). This allows to conclude that in such a specific length the propagated signal shows an amplification. We evince the powerful feature of metasurface that allows to fully control the impinging signal.

In order to show the effect of α on the attenuation, in Fig. 5 we present numerical results in case of a metasurface of length $r = 1$ m, and for $\mathrm{Re}[\alpha] = [0.1, 0.3, 0.6]$. We notice that for increasing $\mathrm{Re}[\alpha]$ the attenuation is decreasing, with short dynamics. Specifically, in Fig. 5(a) we obtain a peak of attenuation of ≈ 30 [dB], while this peak reduces to ≈ 15 [dB] for $\mathrm{Re}[\alpha] = 0.3$ as depicted in Fig. 5(b). Again, we observe that increasing $\mathrm{Im}[\alpha]$ provides fluctuations to attenuation.

Other obtained results depict the attenuation versus the frequency in the THz band. This behavior is obtained by considering $Z_{load} = 1/(j\omega C)$, where C is the load capacitance $[pF]$ and $\omega = 2\pi f$, with f [THz] as the frequency. Similar consideration can be obtained in case of a different behavior of Z_{load} (*e.g.*, $Z_{load} = j\omega L$, with L as the load inductance). Differently from Fig. 4 and Fig. 5, where we observe a dynamic behavior of attenuation, in Fig. 6 the

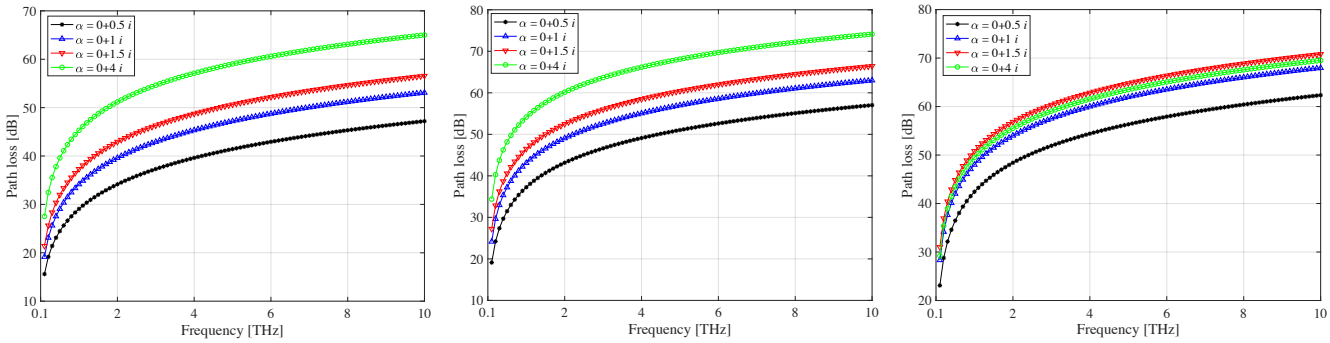

Fig. 6. Attenuation behavior versus the frequency in case of $Z_{load} = 1/(j\omega C)$ with $C = 50pF$, and for different values of α, in case of different metasurface length [m] set to (a) $r = 0.01$, (b) $r = 0.1$, and (c) $r = 0.3$.

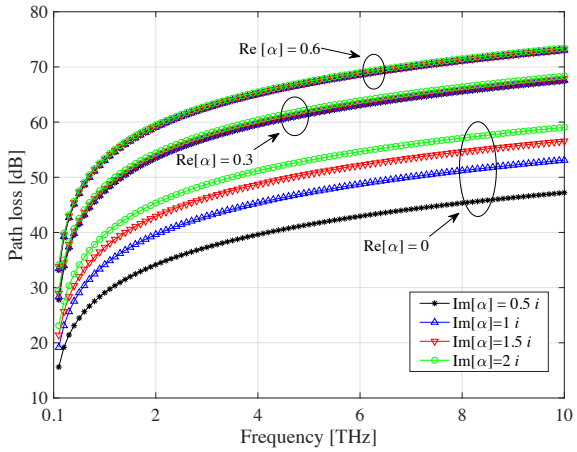

Fig. 7. Attenuation behavior versus the frequency in case of $Z_{load} = 1/(j\omega C)$ with $C = 50pF$, and for different values of $\mathrm{Re}[\alpha]$, in case of $r = 0.01$ m.

attenuation shows its typical trend, with increasing values with the frequency. This occurs for a fixed metasurface length, and for increasing lengths the attenuation curves tend to overlap to each others. Finally, for comparison purpose Fig. 7 presents the attenuation in case of different values of $\mathrm{Re}[\alpha]$. Notice that for increasing $\mathrm{Re}[\alpha]$, the attenuation increases and curves overlap.

V. Conclusions

In this work, a generic tool to model, design and realize curvilinear metasurface-based structures has been presented. The proposed approach exploits the link between Field and Circuit theory to create a robust relation between arbitrary shape surfaces and their material properties, in order to obtain a simultaneous control of amplitude and phase of the wave.

The method has been verified for invisibility applications where it has been shown how simulation and theoretical results match very well. Moreover, the proposed approach has been proven for THz band communications, where it has been show how the amplitude and phase of THz waves can be manipulated before being transmitted on air. Based on the encouraging results, we aim to further develop a complete THz-based wireless communication system based on such a kind metasurface.

References

[1] C. Liaskos, S. Nie, A. Tsioliaridou, A. Pitsillides, S. Ioannidis, and I. Akyildiz, "A New Wireless Communication Paradigm through Software-controlled Metasurfaces," *IEEE Communications Magazine*, vol. 56, no. 9, pp. 162–169, 2018.

[2] C. Liaskos, A. Tsioliaridou, A. Pitsillides, S. Ioannidis, and I. Akyildiz, "Using any Surface to Realize a New Paradigm for Wireless Communications," *Communications of the ACM*, vol. 61, no. 11, pp. 30–33, 2018.

[3] Y. Lee, S.-J. Kim, H. Park, and B. Lee, "Metamaterials and Metasurfaces for Sensor Applications," *Sensors*, vol. 79, no. 1726, 2017.

[4] N. Zheludev and Y. Kivshar, "From metamaterials to metadevices," *Nature Materials*, vol. 11, pp. 917 – 924, 2012.

[5] A. Shaltout, J. Kim, A. Boltasseva, V. Shalaev, and A. Kildishev, "Ultrathin and multicolour optical cavities with embedded metasurfaces," *Nature Communications*, vol. 9, no. 2673, 2018.

[6] Z. Qi, N. Matsuda, K. Itoh, M. Murabayashi, and C. R. Lavers, "A Design for Improving the Sensitivity of a Mach-Zehnder Interferometer to Chemical and Biological Measurands," *Sens. Actuators B*, vol. 81, pp. 254 – 258, 2002.

[7] F. Dell'Olio and V. M. N. Passaro, "Optical sensing by optimized silicon slot waveguides," *Optics Express*, vol. 15, pp. 4977–4993, 2007.

[8] G. Veldhuis, J. H. Berends, R. G. Heideman, and P. V. Lambeck, "An integrated optical Bragg reflector used as a chemo-optical sensor," *Pure Appl. Opt.*, vol. 7, pp. 23–26, 1998.

[9] I. L. Y. Li, C. D. Giovampaola, and N. Engheta, "Waveguide metatronics: Lumped circuitry based on structural dispersion," *Science Advances*, vol. 12, no. 6, 2016.

[10] T. J. Yen, W. J. Padilla, N. Fang, D. C. Vier, D. R. Smith, J. B. Pendry, D. N. Basov, and X. Zhang, "Terahertz magnetic response from artificial materials," *Science*, vol. 303, pp. 1494–1496, 2004.

[11] F. Monticone and A. Alú, "Metamaterials and plasmonics: From nanoparticles to nanoantenna arrays, metasurfaces, and metamaterials," *Chin. Phys. B*, vol. 23, 2014.

[12] X. Ni, A. V. Kildishev, and V. M. Shalaev, "Metasurface holograms for visible light," *Nat. Commun.*, vol. 61, no. 11, pp. 30–33, 2018.

[13] L. La Spada and T. M. McManus and A. Dyke and S. Haq and L. Zhang and Q. Cheng and Y. Hao, "Surface Wave Cloak from Graded Refractive Index Nanocomposites," *Scientific Reports*, vol. 6, no. 29363, 2016.

[14] C. A. Balanis, *Advanced engineering electromagnetics*. Wiley, 2012.

[15] L. L. Spada, F. Bilotti, and L. Vegni, "Metamaterial-based Sensor Design working in Infrared Frequency Range," *Progress In Electromagnetics Research*, vol. 34, pp. 205–223, 2011.

[16] A. M. Vegni and V. Loscrí, "Analysis of the Chirality Effects on the Capacity of Wireless Communication Systems in the THz band," *IEEE Transactions on Wireless Communications*, vol. 16, no. 12, pp. 7848–7858, 2017.